Properties of graphite at melting from multilayer thermodynamic integration

F. Colonna,[1,*] J. H. Los,[2,3] A. Fasolino,[2,1,†] and E. J. Meijer[1,‡]
[1]*Van' t Hoff Institute for Molecular Sciences and Amsterdam Center for Multiscale Modeling, University of Amsterdam, Nieuwe Achtergracht 166, 1018 WV Amsterdam, The Netherlands*
[2]*Institute for Molecules and Materials, Radboud University Nijmegen, Heyendaalseweg 135, 6525 AJ Nijmegen, The Netherlands*
[3]*LRC Méso CMLA, École Normale Supérieure Cachan, 61 avenue du Président Wilson, 94235 Cachan Cedex, France*
(Received 17 July 2009; published 2 October 2009)

Although the melting of graphite has been experimentally investigated for a long time, there is still much debate on the graphite melting properties, as studies show significant discrepancies. We calculate the melting line by means of LCBOPII, a state-of-the-art interaction potential for carbon. To this purpose, we developed a generalized thermodynamic integration scheme, suitable for layered crystals. We also investigate the structure of liquid carbon around the coexistence line, including the undercooled region, as well as its dynamic properties in a wide range of temperatures.

DOI: 10.1103/PhysRevB.80.134103 PACS number(s): 34.20.Cf, 61.20.Ja, 64.70.−p

I. INTRODUCTION

Graphite is the most stable carbon (C) allotrope at ambient condition. It is a strongly anisotropic crystal that consist of layers of sp^2-bonded carbon atoms arranged in a hexagonal structure. The sheets are stacked mostly in an ABAB fashion. While the in-plane bonds are very strong, the interactions among the layers are relatively weak.

A detailed microscopic understanding of the properties of graphite is relevant for nanotechnology, material science, and geophysics. Despite the fact that graphite has been investigated for decades employing a host of different theoretical[1–4] and experimental methods (see Refs. 5 and 6 for a review), there is still much debate on its melting properties. The experimental estimates for the melting line are scattered over a range of 3700–5000 K.

In this paper, we report a computational study of the melting line of graphite using a state-of-the-art atomistic model. We determined the graphite melting line by free energy calculations and characterized the properties of the liquid phase near the melting line, including the undercooled region. This knowledge is important to understand the formation mechanism of carbon-based nanostructures.

Realistic modeling of the melting of graphite requires an accurate description of the interatomic interactions in combination with a precise evaluation of the relative free energies of the graphite and liquid phase. Presently, density functional theory (DFT)-based models incorporating weak long-range interactions[7–11] would provide the best approach to model the interatomic interactions. However, when combined with free energy calculations this approach is prohibitively expensive.

A viable alternative is employing an accurate empirical description of the interatomic interactions. We used the empirical "long-range carbon bond order potential" (LCBOP) that incorporates long-range dispersive interactions, and accurately describes carbon properties for a wide range of structures and conditions. The present work specifically focuses on the properties of carbon near the graphite melting line of the LCBOPII model.[12] This potential incorporates significant improvements on the LCBOPI$^+$ version, which was employed to model the carbon phase diagram in our earlier studies.[13,14] The improvements yield a more accurate description of the high-pressure high-temperature liquid,[15] indicating that it may also provide an improved description of graphite melting.

In the finite periodic systems employed in simulations of graphite, the layers often show sliding due the weak interlayer interaction. The presence of sliding layers requires a dedicated method to determine the free energy of the graphite phase.[16] We provide a generalization of the Frenkel-Ladd free-energy method[17,18] to deal with crystalline systems that show interlayer sliding. In addition to application to graphite and other layered crystalline materials like *BN* and $MoSe_2$, this extension of the Frenkel-Ladd method is also applicable for free energy calculations of other important types of weakly coupled structures, such as multiwalled nanotubes, onion-like fullerenes, or arrays of nanotubes.

II. METHODS

A. Models and simulation methods

We performed simulations employing both the empirical bond-order potential LCBOPII and a DFT based description of the interatomic interactions.

For the LCBOPII model both Monte Carlo (MC) and molecular dynamics (MD) simulations were carried out. In these simulations, the systems consisted typically of 100–300 particles in a periodically replicated cell with rectangular symmetry. MC simulations were performed both at constant density (NVT) and constant pressure (NpT), where the pressure was imposed by (anisotropic) volume changes. In the NVT MD simulations the temperature was imposed by a Nosé thermostat. The MD simulations were performed using the STAMP package.[19]

The DFT-based simulations were performed using the Car-Parrinello molecular dynamics scheme[20] as implemented in the CPMD software package.[21] In these *ab initio* molecular dynamics (AIMD) simulations the electronic structure was obtained from the Kohn-Sham formulation[22] of DFT,[23] where we employed the gradient-corrected Becke-Perdew

functional.[24] The Kohn-Sham orbitals are expanded in plane waves with an energy cutoff of 35 Ry. Only valence electrons are considered explicitly, with a semilocal norm-conserving Martins-Troullier pseudo potential[25] taking into account the interactions between the core and valence electrons. The cutoff radius for the carbon pseudopotential is taken 0.635 Å. The fictitious mass associated with the plane-wave coefficients is set 100 a.u., allowing for a time step of 0.0484 fs in the numerical integration of the equations of motion. Liquid carbon shows metallic behavior in our AIMD simulations. For metallic systems, the Car-Parrinello method requires the electronic degrees of freedom to be coupled to a thermostat.[26] Here, we coupled a Nosé-Hoover chain thermostat to the electronic degrees of freedom with a target energy of 0.015 eV and a coupling frequency of 15000 cm^{-1}.

B. Thermodynamic integration

The Helmoltz free energy in the canonical NVT ensemble is given by

$$F(N,V,T) = -\frac{1}{\beta}\ln Z(N,V,T) \tag{1}$$

where $Z(N,V,T)$ is the partition function defined as

$$Z(N,V,T) = C_N \int e^{-\beta H(\mathbf{r}^N,\mathbf{p}^N)} d\mathbf{r}^N d\mathbf{p}^N \tag{2}$$

with $C_N = \frac{1}{N!}\frac{1}{h^{3N}}$, $\beta = \frac{1}{k_B T}$, and $H(\mathbf{r}^N,\mathbf{p}^N) = \Sigma_{i=1}^N \frac{p_i^2}{2m} + U(\mathbf{r}_1,\ldots\mathbf{r}_N)$ the Hamiltonian of a single component system.

The factorial $N!$ in C_N takes into account the indistinguishability of the particles; in model-systems such as the "Einstein Crystal" the particles are distinguishable and $C_N = \frac{1}{h^{3N}}$ should be used.

The partition function can be factorized in a kinetic and a configurational part, denoted by $P(N,V,T)$ and $Q(N,V,T)$, respectively:

$$P(N,V,T) = C_N \int e^{-\beta\Sigma_{i=1}^N p_i^2/2m} d\mathbf{p}^N = C_N \left(\frac{2\pi m}{\beta}\right)^{3N/2}$$

$$Q(N,V,T) = \int_V e^{-\beta U(\mathbf{r}_1,\ldots\mathbf{r}_N)} d\mathbf{r}^N. \tag{3}$$

The configurational part of the free energy ($\tilde{F}$) is defined by

$$\tilde{F}(N,V,T) = -\frac{1}{\beta}\ln Q(N,V,T). \tag{4}$$

At fixed temperature, the free energy difference ΔF of two systems (*I* and *II*, e.g. two different volumes or interaction potentials) is determined by the difference in the configurational part of the free energies: $\Delta F = \Delta\tilde{F}$.

The free energy of a state point in the phase diagram can be obtained by employing the thermodynamic integration technique. It consists of two steps. First a reference model-system with known free energy is chosen such that it has structural properties similar to those of the state point under consideration. For a liquid state point, the Lennard-Jones (LJ) system may serve as a reference system, since an accurate parametrized expression for the free energy has been determined by computer simulations.[27] A convenient reference system for a solid is the "Einstein Crystal" (EC)[28] with the corresponding lattice structure. Its free energy can be evaluated analytically. The potential energy function of an EC is defined by the potential $U_{\mathrm{EC}}(\mathbf{r}_1,\ldots,\mathbf{r}_N) = \Sigma_{i=1}^N [\alpha_x(x_i - x_i^0)^2 + \alpha_y(y_i - y_i^0)^2 + \alpha_z(z_i - z_i^0)^2]$ where $\alpha_{x,y,z}$ are the spring force constants for vibrations around the reference positions $\mathbf{r}_i^0$. The set of points $\{\mathbf{r}_0^i\}_{i=1\ldots N}$ is usually chosen to be the equilibrium lattice of the crystal to be simulated.

The second step of thermodynamic integration is to transform the interaction potential of the reference system U_{REF} into that of the state point under consideration, and measure the free-energy change associated with the transformation. This can be achieved by making use of a parametric potential $U_\lambda(\mathbf{r}_1,\ldots\mathbf{r}_N)$ that coincides with the reference potential for $\lambda = 0$ and with that of the state point under consideration for $\lambda = 1$,

$$U_\lambda = \lambda U + (1-\lambda)U_{REF}. \tag{5}$$

Then, the final configurational free energy can be expressed as:[28]

$$\tilde{F} = \tilde{F}_{REF} + \int_{\lambda=0}^{\lambda=1} \langle \Delta U\rangle_\lambda d\lambda, \tag{6}$$

where $\Delta U = \langle U_{REF} - U\rangle_\lambda$, and $\langle\ldots\rangle_\lambda$ is the canonical average with the interaction potential U_λ.

In the practical implementation with the EC reference system, one has to take care of the following. In the limit of vanishing coupling to the EC lattice points ($\lambda = 1$), the system as a whole is free to translate, stretching the springs to any length and leading to a divergence of $\langle U_{REF} - U\rangle_{\lambda=1}$ in Eq. (6).

To avoid this problem the EC lattice and the equilibrium lattice of the crystal should be coupled. This can be achieved by imposing the center-of-mass (CM) of the system to remain equal to the one of the EC lattice (CM^0) [17,18] during the simulation. The configurational free energy of a system with potential energy U, calculated by integrating from an EC with $\alpha = \alpha_x = \alpha_y = \alpha_z$ is then given by[18]

$$\frac{\beta\tilde{F}}{N} = \frac{3}{2}\ln\left(\frac{\alpha\beta}{\pi}\right) + \beta\int_0^1 \langle \Delta u\rangle_\lambda^* d\lambda - \frac{1}{N}\left[\frac{3}{2}\ln\left(\frac{\alpha\beta}{\pi}\right) - \ln(V_{PC})\right]. \tag{7}$$

Here, V_{PC} is the volume of the primitive cell (PC), $u = U/N$ is the potential energy per particle, and the superscript * indicates that the averages are evaluated in the canonical ensemble with the constraint $CM = CM^0$. The first term is the free energy of the reference EC; the second term specifies the free-energy change upon transformation from the EC crystal to the system under consideration; the third one yields the correction associated with the constraint on the CM. Note that the latter term yields a finite-size correction that vanishes in the thermodynamic limit.

C. Multi-reference method

Performing simulations of graphite at high temperatures, we observe a sliding of the graphite planes along each other. This effect is due to the weakness of the interaction between nearby planes and to the finite size of the sample. In this case, relevant for graphite and similar layered systems, the EC method of Refs. 17 and 18 outlined in Sec. II B has to be amended.[14,16] Since layers can slide in opposite directions by any amount keeping CM and CM^0 equal, $\langle U_{REF}\rangle$ is unbound in the limit of vanishing coupling to the EC lattice points ($\lambda=0$), and the integrand in Eq. (6) is ill defined.

We propose an EC free-energy method for crystalline layered systems that avoids this divergence in the vanishing EC limit and allows for accurate free energy calculations in layered crystals. We also provide an expression to evaluate the finite size correction to the free energy due to the sliding of the EC planes that generalizes Eq. (7).

The philosophy is to use a set of independent EC sublattices and to couple each of them to a single graphite sheet, ensuring the maximal structural resemblance. We allow the reference planes to move independently only in the in-plane (xy) direction, while in the z direction the reference positions of all planes are displaced by the same amounts, having therefore a fixed inter-planar distance. We consider a graphite structure made of M sheets s_j with $j=1\ldots M$. The CM^0 of the reference planes follows the CM of the corresponding graphitic sheet. The in-plane translations of the references are then $t_j^x=\frac{1}{n}\Sigma_{i\in s_j}x_{i,j}$ and $t_j^y=\frac{1}{n}\Sigma_{i\in s_j}y_{i,j}$, where $x_{i,j}(y_{i,j})$ indicates the $x(y)$ coordinate of atom i in plane j and $n=N/M$ is the number of particles of each sheet. In the out-of-plane direction the reference planes are all displaced by the same amount, in order to follow the position of the total center of mass: $t^z=\frac{1}{N}\Sigma_{i=1}^N z_i$.

As a result, the expression for the EC interaction is:

$$U_{\mathrm{EC}}(\mathbf{r}^N;\mathbf{t}^M)=\sum_{j=1}^{M}\sum_{i=1}^{n}[\alpha_x(x_{i,j}-x_{i,j}^0-t_j^x)^2+\alpha_y(y_{i,j}-y_{i,j}^0-t_j^y)^2+\alpha_z(z_{i,j}-z_{i,j}^0-t^z)^2] \tag{8}$$

where, t_j^x,t_j^y,t^z are functions of the positions $\mathbf{r}_{i,j}$. The configurational partition function

$$Q_\lambda=\int e^{-\beta U_\lambda(\mathbf{r}^N)}\mathrm{d}\mathbf{r}^N \tag{9}$$

coincides for $\lambda=1$ with the canonical partition function Eq. (3). In the case of graphite it is useful to consider an EC with springs of different strength in the xy and in the z direction: $\alpha_{xy}=\alpha_x=\alpha_y$ and α_z. For $\lambda=0$ it is possible to evaluate the integral analytically, obtaining

$$\begin{aligned}Q_{\lambda=0}^*&=\left[\left(\frac{\pi}{\alpha_{xy}\beta}\right)^N(S_{xy})^M\left(\frac{\alpha_{xy}\beta}{\pi}\right)^M n^M\right]\left[\left(\frac{\pi}{\alpha_z\beta}\right)^{N/2}L_z\left(\frac{\alpha_z\beta}{\pi}\right)^{1/2}N^{1/2}\right]\\&=V_{PC}Q_{\mathrm{EC}}^{\mathrm{CM}}\left[(S_{xy})^{(M-1)}\left(\frac{\alpha_{xy}\beta}{\pi}\right)^{M-1}(n)^M N^{-1}\right]\end{aligned} \tag{10}$$

where $Q_{\mathrm{EC}}^{\mathrm{CM}}=(\frac{\pi}{\beta})^{3(N-1)/2}[\frac{1}{\alpha_{xy}}(\frac{1}{\alpha_z})^{1/2}]^{(N-1)}N^{3/2}$ (Ref. 18) is the configurational partition function of the EC with the global CM equal to CM^0, and S_{xy} is the surface of the two-dimensional (2D) in-plane primitive cell. The factor in square brackets in the last line of Eq. (10) results from the presence of the multiple reference planes.

By inserting $\tilde{F}_{REF}=-\frac{1}{\beta}\ln(Q_{\lambda=0}^*)$ in Eq. (6), we arrive at the following expression for the configurational free energy of graphite:

$$\begin{aligned}\frac{\beta\tilde{F}}{N}&=\ln\left(\frac{\alpha_{xy}\beta}{\pi}\right)+\frac{1}{2}\ln\left(\frac{\alpha_z\beta}{\pi}\right)+\int_0^1\langle\Delta u\rangle_\lambda\mathrm{d}\lambda-\frac{1}{N}\left[\ln\left(\frac{\alpha_{xy}\beta}{\pi}\right)+\frac{1}{2}\ln\left(\frac{\alpha_z\beta}{\pi}\right)+\ln(V_{PC})\right]\\&\quad-\frac{1}{N}\left\{(M-1)\left[\ln\left(\frac{\alpha_{xy}\beta}{2\pi}\right)+\ln(S_{xy})+\ln(N)\right]-M\ln(M)\right\}.\end{aligned} \tag{11}$$

We collected the finite-size corrections in two different square brackets: the first corresponds to the correction in Eq. (7), while the second contains the correction due to the sliding of the EC planes. The latter vanishes for $M=1$, so that Eq. (7) is recovered. Notice that in our approach this term vanishes in the thermodynamic limit as slow as $\ln(N)/N^{2/3}$, and it is therefore important to take it into account correctly.

It is important to note that the above outlined multi-reference approach can be applied to other weakly bounded complex systems that have subsystems showing sliding or rotation relative to each other. This class may include onion-like structures and nanotube arrays.

D. Coexistence

In a one-component system the coexistence line is the locus of the points (T_c,p_c) where the difference of the Gibbs free energy $G(N,p,T)=F(N,V,T)+pV$ between the two

phases vanishes. In the previous section, we have outlined how to obtain the free energy by thermodynamic integration. Starting from a state point near coexistence, the temperature dependence of the difference in Gibbs free energy can be obtained by integrating

$$\frac{\partial}{\partial_\beta}[\beta\Delta G(N,p,T)] = \langle \Delta E + p\Delta V\rangle_{NpT}. \tag{12}$$

The coexistence temperature T_c can then be located as the temperature where $\Delta G=0$.

Once a single coexistence point (T_c,p_c) is known, one can trace the coexistence line by integrating the Clausius-Clapeyron equation[29]

$$\frac{dT_c}{dp_c} = \frac{T_c\Delta V_c}{\langle \Delta E_c + p_c\Delta V_c\rangle} \tag{13}$$

where ΔV_c and ΔE_c are the volume and energy differences between the two phases at the point (T_c,p_c). We integrated Eq. (13) with the trapezoidal predictor-corrector scheme proposed by Kofke.[29] We used an integration step of $\delta p=1$ GPa. The averages $\langle E\rangle$ and $\langle V\rangle$ were calculated with NpT-MC runs of 5×10^4 MC cycles (one MC cycle corresponds to N particle moves) following equilibration runs of 1×10^4 MC cycles. In the case of graphite we performed anisotropic volume moves along the Cartesian directions.

III. RESULTS

A. Melting temperature at 2 GPa

As a starting point to trace the melting line for the LCBOPII model, we determined the coexistence point at the pressure of 2 GPa. This is the lowest pressure where a direct comparison with the results for the LCBOPI$^+$ model is possible. The thermodynamic integration of the graphite and of the liquid state point was performed at T=4250 K.[30]

The accuracy of the thermodynamic integration is influenced by the choice of the parameters of the reference potentials, i.e., the σ and the ϵ of the LJ potential and the α_{xy}, α_z of the EC. The overlap of the configuration space accessed by the reference and the LCBOPII systems should be as large as possible, and the conversion from one system to another as smooth as possible. The reference system for the free energy calculation of the liquid state was taken as a system with a cut and shifted LJ potential, with cutoff $r_c=4\sigma$. The free energy of this LJ liquid has been accurately parametrized in Ref. 27. The values of ϵ and σ were chosen in the supercritical domain, and such that there is a maximal similarity of the local structure of the LJ and LCBOPII liquid by matching the position of the first peak of the radial distribution function $g(r)$. This yields a value of $\epsilon=0.2$ eV Å^{-2}, $\sigma=1.3$ Å.

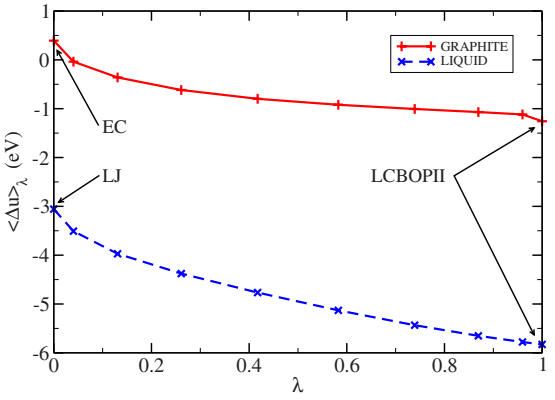

FIG. 1. (Color online) Behavior of $\langle \Delta u\rangle_\lambda$ as a function of λ. The red plus-symbols correspond to the thermodynamic integration of graphite from the multireference EC. Note the absence of any divergence at λ=1, despite the relative sliding of the graphite sheets. The blue crosses correspond to the thermodynamic integration of the liquid. The connecting solid and dashed lines are a guide to the eye. The error bars are smaller than the size of the symbols.

TABLE I. Helmholtz free energies per particle at T=4250 K and volumes corresponding to the average volume at p=2 GPa, associated to the reference systems (λ=0), to the thermodynamic integration and to the final carbon phase (λ=1).

Phase	$\beta F_{\lambda=0}/N$	$\beta\int d\lambda\langle\Delta u\rangle_\lambda$	$\beta F_{\lambda=1}/N$
Graphite	−22.3571	−2.090(0.027)	−24.447(0.027)
Liquid	−11.1963	−13.2517(0.0014)	−24.4480(0.0014)

For graphite, the coupling constants α_{xy} and α_z of the harmonic potential were chosen such that the mean-squared displacement (MSD) around the equilibrium position $\langle\Sigma_{i=1}^N|\mathbf{r}_i-\mathbf{r}_i^0|^2\rangle$ is similar to that of the LCBOPII system. The parameters we used are: $\alpha_{xy}=16$ eV Å^{-2} and $\alpha_z=2$ eV Å^{-2}. The graphite sample in the periodic box consisted of four graphite sheets of 72 particles each. The liquid sample contained 216 particles in a cubic periodic box.

The results are shown in Fig. 1. For every value of λ we run MC simulations of 10^6 MC cycles. Before starting averaging we equilibrated the sample for 10^4 MC cycles. The results of the λ-integration are summarized in Table I.

The results of Table II, where we report the magnitude of the finite-size corrections, clearly show that the effect of the sliding reference is not negligible. The total free energies per particle ($\beta F/N$ in the tables) of the two phases are equal within the error bars. As the pressure is small and the volume per particle v in the two phases is very close, also the difference in the Gibbs free energy turns out to be zero within the error-bar: $\beta(\tilde{G}_{\rm liq}-\tilde{G}_{\rm graph})=\beta\Delta\tilde{F}/N+\beta p\Delta v=0.0010(0.0027)-0.0016(0.0001)=-0.0006(0.0027)$. This small difference in the Gibbs free energy yields a negligible shift down (4 K) of the melting temperature with respect to the temperature of the thermodynamic integration. Our final estimate for the melting temperature at 2 GPa is 4250 K ± 50.

TABLE II. Magnitude of the finite-size correction per particle for the graphite's multilayered thermodynamic integration results reported in Table I.

Ordinary corr.	Sheets corr.	Total corr.
−0.0647	−0.0975	−0.1621

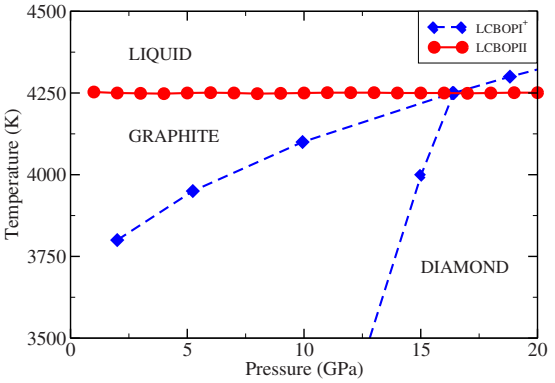

FIG. 2. (Color online) Graphite melting line according to LCBOPII (red dots, solid line), compared to the LCBOPI+ carbon phase diagram (blue diamonds, dashed lines).

B. Melting line

We traced the coexistence line in the interval 1–20 GPa by means of the trapezoidal predictor-corrector scheme (Fig. 2).[29] Note that beyond 16 GPa the stable phase is diamond. Using the numerical details given in Sec. II D, the difference between the "predictor" and the "corrector" estimates was less than 2 K on all points.

The negligible dependence on pressure of the melting temperature is due to the fact that the volumes per particle in the two phases are almost equal [Eq. (13)] over the whole coexistence line, despite the fact that the value decreases by more than 25% (Fig. 3). In the same figure we also plot the volumes per particle for the liquid and for the over-heated graphite at T=4750 K. On this isotherm the difference in volume per particle increased, but becomes only significant for pressures below 6 GPa. Hence, for LCBOPII the volume per particle of graphite is only slightly larger that that of the liquid over a wide range of pressures and temperatures around the melting line.

The experimental melting temperatures are scattered over the interval 3700–5000 K, strongly depending on the details of the experimental apparatus and on the heating rate of the graphite sample.[6] Togaya *et al.*,[31] whose investigation is considered to be the most reliable by Bundy,[5] report a melting line between 4600 K and 4800 K, with a gentle maximum around 5 GPa. However, this is an indirect observation, as the melting temperature is deduced from the measured enthalpy of melting. They measure an enthalpy of melting around 1.23 eV per particle. Taking the difference of enthalpy per particle between the two phases $\Delta E/N+p\Delta V/N$, we found a value of 0.63 ± 0.01 eV at 0 GPa, which decreases linearly to 0.56 ± 0.01 eV at 15 GPa. In a review of 40 years of investigations over this topic, Savvatimskiy[6] conclude that the majority of the reliable estimates give a melting temperature between 4600 and 5000 K. Compared to the LCBOPI+ the melting line shifts to higher temperatures, closer to the experimental values of Ref. 31. In this respect, LCBOPII improves the results of LCBOPI+, even though it probably still underestimates the melting line of a few hundred Kelvin.

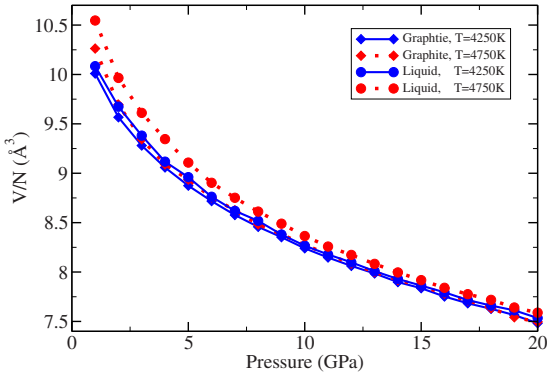

FIG. 3. (Color online) Volume per particle in liquid carbon (circles) and in graphite (diamonds) on the isotherms at T =4250 K (blue solid lines) and T=4750 K (red dashed lines). Error-bars are within the size of the symbols.

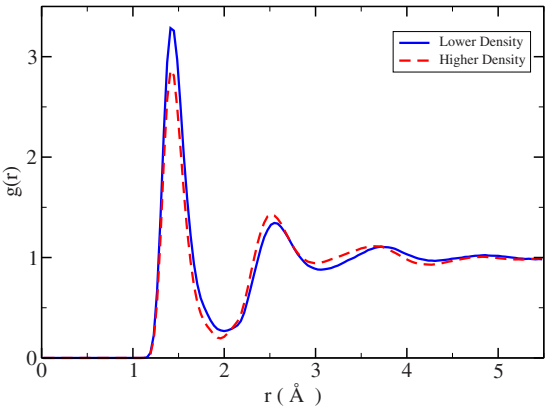

FIG. 4. (Color online) LCBOPII radial distribution functions on the melting line at the densities of 1.94 g cm^{-3} (T=4250 K) and 2.59 g cm^{-3} (T=4250 K) (solid blue and dashed red lines, respectively).

C. Low-density liquid carbon

We analyzed the local structure of liquid carbon for 5 different pressures (0,5,10,15, and 20 GPa) along the melting

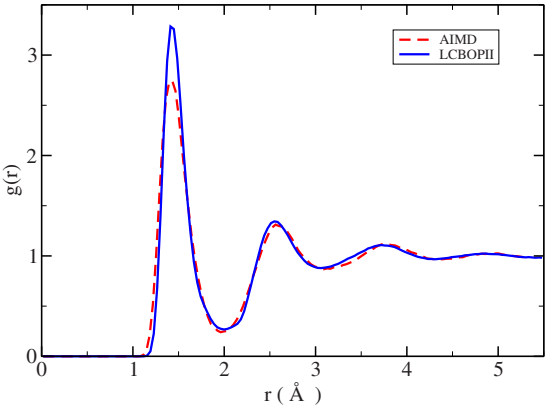

FIG. 5. (Color online) LCBOPII (solid blue) and AIMD (dashed red) radial distribution functions on the melting line (T=4250 K) at the density of 1.94 cm^{-3}.

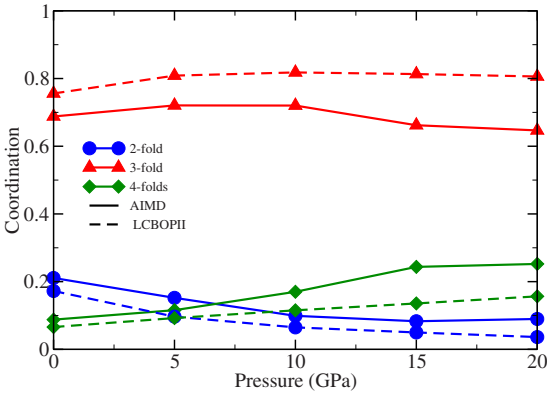

FIG. 6. (Color online) Coordination fractions in the undercooled liquid at T=4000 K. The twofold coordination fractions are represented by circles, the threefold by triangles, and the fourfold by diamond. The one calculated according to LCBOPII are connected by solid lines, the one obtained with ab-initio simulations by dashed ones.

line and in the undercooled liquid at T=4000 K. We also investigated the diffusive behavior of the liquid, performing classical and AIMD simulations up to 7000 K. These are key properties to describe the stability and nucleation of graphite and graphite-related materials or nanostructures. All simulations have been performed in the NVT ensemble. The density has been determined with NpT-MC simulations, in order to reproduce the (LCBOPII) coexistence densities at the selected pressures. The systems consisted of 128 particles in a periodic box, known to be large enough to give a sufficiently accurate description of liquid carbon.[32,33]

1. Local structure

In Fig. 4, we show the radial distribution function $g(r)$ for the LCBOPII liquid along the coexistence line, at two densities. Liquid carbon appears to be very structured. As shown in Fig. 5, the LCBOPII reproduces well the features of the g(r) obtained with AIMD at the same state-points, although

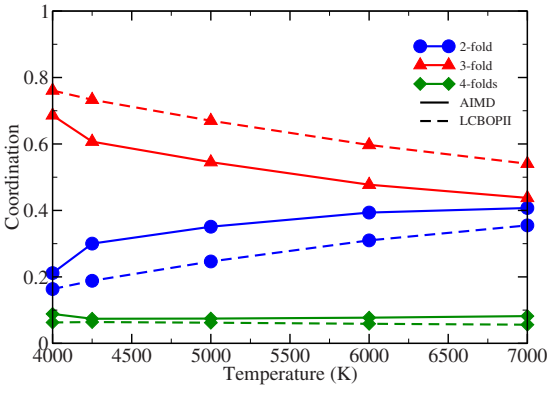

FIG. 7. (Color online) Coordination fractions in the liquid carbon at low density (1.94 g cm^{-3}) as function of the temperature. The legend is the same as in Fig. 6. The AIMD results show that the liquid is mainly threefold coordinated, although the difference between twofold and threefold fractions becomes small around 7000 K. The LCBOPII model is able to reproduce qualitatively the trend.

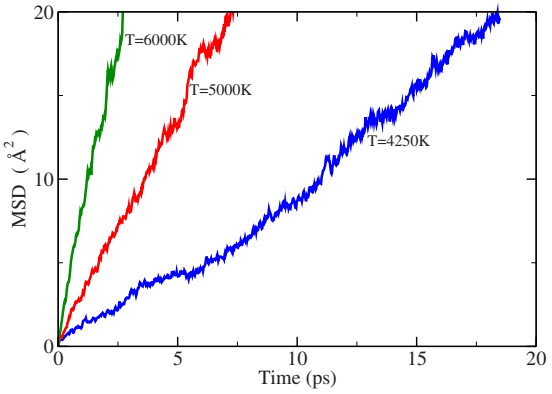

FIG. 8. (Color online) Mean square displacements for the LCBOPII-MD simulations for the temperatures T=4250 K, 5000 K, 6000 K (blue, red, and green lines, respectively) at the density of ρ=1.94 g cm^{-3}. The plot is truncated at the MSD of 20 Å^2.

the first peak is sharper and more pronounced.

Along the melting line and inside the undercooled region, the liquid is mainly threefold coordinated, with smaller fractions of twofold and fourfold coordinated atoms. In Fig. 6 we show the LCBOPII coordination fractions at 4000 K, against the ab-initio benchmarks. The coordination are evaluated according to the definition used in the LCBOPII potential.[12] Compared to the behavior of LCBOPI$^+$ around the coexistence,[34] LCBOPII shows improvements in several respects. Firstly, the fraction of the threefold coordinated atoms is now closer to the one of the benchmarks, although still slightly over estimated. Secondly, the twofold prevails on the fourfold at low pressures, but it disappears as soon as the pressure is increased to a few GPa. LCBOPII reproduces the trend of the *ab initio* benchmarks as the pressure is increased. Increasing the temperature, the threefold fraction decreases and the liquid becomes increasingly twofold, as shown in Fig. 7 for the density of 1.94 g cm^{-3}. LCBOPII is able to reproduce this trend, although at higher temperatures the threefold fraction is slightly over estimated.

2. Diffusive behavior

So far, there is very limited data available on the diffusion in liquid carbon. Galli *et al.*[35] reported a value of the diffusion constant of 2.4×10^{-4} cm^2 s^{-1} obtained with AIMD simulations, at a temperature of 5000 K and a density of 2.0 g cm^{-3}. Later, for the same state-point, Goedecker and Colombo[36] reported a value of 3.5×10^{-4} cm^2 s^{-1} obtained by means of tight-binding MD simulations. Recently, Ghiringhelli *et al.*[13] extrapolated the diffusion coefficient around the melting temperature assuming that liquid carbon is an Arrhenius liquid. Here, we report the results of our investigation on the diffusion of the graphite melt at two densities (1.94 and 2.59 g cm^{-3}). Those corresponds to the density at the temperature of 4000 K and the pressures of 0 GPa and 15 GPa. All MD simulations have lasted long enough to reach (at least) a MSD of 20 Å^2, corresponding to an average particle displacement of about three interatomic distances. In Fig. 8, we report the MSDs for the LCBOPII simulations at the lower density (1.94 g cm^{-3}) and at the temperatures of T=4250 K, 5000 K, and 6000 K.

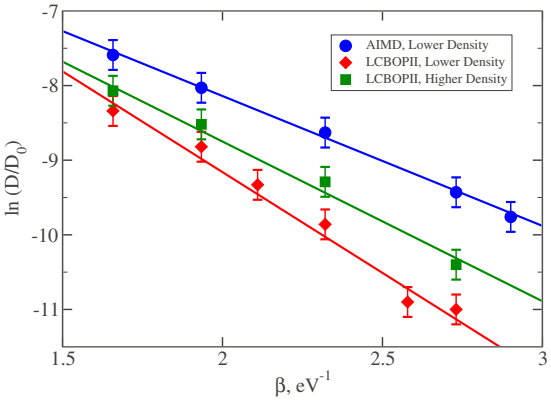

FIG. 9. (Color online) Arrhenius plot of the diffusivity of the liquid carbon at two different densities. The AIMD results at the lower density (1.94 g cm^{-3}) are represented by blue circles, the LCBOPII one by red diamonds. The green squares are the LCBOPII results at the density of 2.59 g cm^{-3}. On the *y*-axis we plot $\ln(D/D_0)$, where $D_0=1$ cm^2 s^{-1}. On the *x*-axis we plot the inverse temperature β for the temperature range 4000 K–7000 K. The lines are the linear fits of the shown data sets. The error bars provide a rough estimate for the statistical accuracy.

For an Arrhenius liquid, it holds that

$$D(T) = Ce^{-E_a/k_BT}, \tag{14}$$

where E_a is interpreted as the activation energy associated to the diffusion and C is a kinetic prefactor. In Fig. 9, we plot the logarithm of the LCBOPII and AIMD diffusion coefficients against the inverse temperature β. By fitting those data, we get an estimate for E_a, reported in Table III.

As compared with AIMD, LCBOPII overestimates the activation barrier for the diffusion, resulting in a somewhat slower dynamics at temperatures around the melting one. The diffusion coefficient is very sensitive to the details of the interaction, and can change with temperature by several orders of magnitude. LCBOPII is able to reproduce the Arrhenius behavior shown by the AIMD, and to predict the right order of magnitude for the diffusion coefficient, although the dynamic seems systematically slower. This observation could be connected to the small differences in the local structure of the two liquids.

IV. CONCLUSIONS

For weakly bounded layered systems, it is hard to get an accurate estimate of the free energy with ordinary thermodynamic integration schemes, because the sliding of the sheets results in a strongly divergent integral. We propose a general multireference approach that is able to overcome this problem, allowing for precise evaluation of free energies for complex systems composed by weakly bound subsystems. We use this technique to calculate the melting line of graphite, as described by the LCBOPII model of interaction. We show that in this case the sliding of the sheets gives a nonnegligible finite-size contribution to the absolute free energy.

The calculated graphite melting temperature for LCBOPII is 4250 ± 50 K for pressures up to 20 GPa. Although experimental data for the melting temperature ranges from 3700 K to over 5000 K, recent reviews consider melting temperatures between 4600 and 5000 K to be the most reliable with overall a limited pressure dependence of the melting temperature. Hence, LCBOPII reproduced well the latter experimental observation and predicts a melting temperature only slightly below (~10%) the most reliable experimental values. It improves significantly over the LCBOPI+phase diagram, especially at low pressure.

We also investigated the structure and the diffusive behavior of the liquid, comparing them to *ab initio* benchmarks. The structure of the liquid is in good agreement with the *ab initio* benchmarks around and above the melting temperature. The diffusion follows an Arrhenius behavior, giving a qualitatively correct description, as compared with the *ab initio* benchmarks.

The capability of LCBOPII to describe thermodynamical, structural, and dynamic features of the liquid carbon, makes it suitable for the study of the stability and growth of graphite-related nanostructures.

TABLE III. Results of the linear fit of the Arrhenius plots $\ln(D/D_0)=\ln(C/D_0)-\beta E_a$ reported in Fig. 9. $D_0=1$ cm^2 s^{-1}

Model	ρ (g cm^{-3})	E_a (eV)	$\ln(C/D_0)$
LCBOPII	2.59	2.2 ± 0.2	-4.38 ± 0.37
LCBOPII	1.94	2.7 ± 0.2	-3.76 ± 0.42
AIMD	1.94	1.74 ± 0.06	-4.66 ± 0.13

ACKNOWLEDGMENTS

We gratefully acknowledge useful discussions with N. Pineau (CEA/DAM). We acknowledge financial support from the EuroSim Marie-Curie EST program.

*f.colonna@uva.nl
†a.fasolino@science.ru.nl
‡e.j.meijer@uva.nl

[1] P. L. Silvestrelli and M. Parrinello, J. Appl. Phys. **83**, 2478 (1998).
[2] J. N. Glosli and F. H. Ree, Phys. Rev. Lett. **82**, 4659 (1999).
[3] L. E. Fried and W. M. Howard, Phys. Rev. B **61**, 8734 (2000).
[4] L. D. Son, G. M. Rusakov, and N. N. Katkov, Dokl. Phys. **51**, 56 (2006).
[5] F. P. Bundy, W. A. Bassett, M. S. Weathers, R. J. Hemley, H. K. Mao, and A. F. Goncharov, Carbon **34**, 141 (1996).
[6] A. I. Savvatimskiy, Carbon **43**, 1115 (2005).
[7] H. Rydberg, M. Dion, N. Jacobson, E. Schroder, P. Hyldgaard, S. I. Simak, D. C. Langreth, and B. I. Lundqvist, Phys. Rev. Lett.

91, 126402 (2003).
[8] M. Dion, H. Rydberg, E. Schroder, D. C. Langreth, and B. I. Lundqvist, Phys. Rev. Lett. **92**, 246401 (2004).
[9] M. Hasegawa and K. Nishidate, Phys. Rev. B **70**, 205431 (2004).
[10] M. Hasegawa, K. Nishidate, and H. Iyetomi, Phys. Rev. B **76**, 115424 (2007).
[11] Y. J. Dappe, M. A. Basanta, F. Flores, and J. Ortega, Phys. Rev. B **74**, 205434 (2006).
[12] J. H. Los, L. M. Ghiringhelli, E. J. Meijer, and A. Fasolino, Phys. Rev. B **72**, 214102 (2005).
[13] L. M. Ghiringhelli, C. Valeriani, J. H. Los, E. J. Meijer, A. Fasolino, and D. Frenkel, Mol. Phys. **106**, 2011 (2008).
[14] L. M. Ghiringhelli, J. H. Los, E. J. Meijer, A. Fasolino, and D. Frenkel, Phys. Rev. Lett. **94**, 145701 (2005).
[15] L. M. Ghiringhelli, J. H. Los, A. Fasolino, and E. J. Meijer, Phys. Rev. B **72**, 214103 (2005).
[16] L. M. Ghiringhelli, Ph.D. Thesis, University of Amsterdam, The Netherlands, 2006.
[17] D. Frenkel and A. J. C. Ladd, J. Chem. Phys. **81**, 3188 (1984).
[18] J. M. Polson, E. Trizac, S. Pronk, and D. Frenkel, J. Chem. Phys. **112**, 5339 (2000).
[19] STAMP: Parallel molecular dynamics code developed at CEA (France).
[20] R. Car and M. Parrinello, Phys. Rev. Lett. **55**, 2471 (1985).
[21] CPMD 3.7.1, Copyright IBM Corp 1990–2004, Copyright MPI für Festkörperforschung Stuttgart 1997–2001.
[22] W. Kohn and L. J. Sham, Phys. Rev. **140**, A1133 (1965).
[23] P. Hohenberg and W. Kohn, Phys. Rev. **136**, B864 (1964).
[24] A. D. Becke, Phys. Rev. A **38**, 3098 (1988); J. P. Perdew, Phys. Rev. B **33**, 8822 (1986).
[25] N. Troullier and J. L. Martins, Phys. Rev. B **43**, 1993 (1991).
[26] P. E. Blöchl and M. Parrinello, Phys. Rev. B **45**, 9413 (1992).
[27] J. K. Johnson, J. A. Zollweg, and K. E. Gubbins, Mol. Phys. **78**, 591 (1993).
[28] D. Frenkel and B. Smit, *Understanding Molecular Simulations*, 2nd ed. (Academic Press, San Diego, CA, 2002).
[29] D. A. Kofke, J. Chem. Phys. **98**, 4149 (1993).
[30] A preliminary calculation at $T=4000$ K with limited accuracy showed the coexistence temperature to be near $T=4250$ K.
[31] M. Togaya, S. Sugiyama, and E. Mizuhara, in *High Pressure Science and Technology*, edited by S. C. Schmid, J. W. Shaner, G. A. Samara, and M. Ross (American Institute of Physics, New York, 1994), p. 255; M. Togaya, Phys. Rev. Lett. **79**, 2474 (1997).
[32] A. A. Correa, S. A. Bonev, and G. Galli, Proc. Natl. Acad. Sci. U.S.A. **103**, 1204 (2006).
[33] X. Wang, S. Scandolo, and R. Car, Phys. Rev. Lett. **95**, 185701 (2005).
[34] L. M. Ghiringhelli, J. H. Los, E. J. Meijer, A. Fasolino, and D. Frenkel, J. Phys.: Condens. Matter **17**, S3619 (2005).
[35] G. Galli, R. M. Martin, R. Car, and M. Parrinello, Phys. Rev. B **42**, 7470 (1990).
[36] S. Goedecker and L. Colombo, Phys. Rev. Lett. **73**, 122 (1994).